Effect of ambient gas and crystal features on Doppler ultrasound twinkling of pathological mineralizations

Eric Rokni,[1,a] and Julianna C. Simon[1]

[1] *Graduate Program in Acoustics, The Pennsylvania State University, University Park, PA, 16802, USA*

Color Doppler twinkling on kidney stones and other pathological mineralizations is theorized to arise from stable microbubbles, which suggests twinkling will be sensitive to ambient gas. Here, cholesterol, calcium phosphate, and uric acid crystals were imaged with ultrasound in water while varying oxygen, carbon dioxide, and nitrogen levels. Twinkling was found to increase on cholesterol in elevated oxygen, cholesterol and calcium phosphate in elevated carbon dioxide, and no crystals in elevated nitrogen. These results support the crevice microbubble theory of twinkling and suggest gases may be varied to enhance twinkling on some mineralizations.

[a] Email: roknieric@gmail.com

I. INTRODUCTION

Minerals can form in the body from pathologies that cause either an oversaturation of chemicals (e.g. kidney stones or gout) or cellular deposition (e.g. heterotopic ossification or breast microcalcifications).[1-4] In addition to kidney stones which can form from a variety of chemicals, mineralizations can form from calcium phosphate as heterotopic ossification or breast microcalcifications, cholesterol as atherosclerosis or gallstones, or uric acid as gout. Current methods for detecting pathological mineralizations either expose patients to ionizing radiation, are expensive, or have low sensitivities.[1,3] The color Doppler ultrasound twinkling artifact, or twinkling, can aid in the detection of pathological mineralizations and is theorized to arise from ultrasound scattering off microbubbles stabilized in crevices.[5,6] Pathological mineralizations form with different crystal structures in a variety of environments (e.g. urine, synovial fluid, soft tissue) which can influence how bubbles form.[7] Similarly, dissolved gases in the surrounding environment will also influence the bubbles that form on mineralizations, which would, in turn, affect twinkling. The goal of this paper is to determine how crystal microstructures and gas affect twinkling on lab-grown crystals.

Twinkling was first noted on kidney stones in 1996[8] but has since been found on breast microcalcifications, encrusted catheters, and, more recently, crystals grown *in vitro*.[7,9,10] Twinkling can improve the sensitivity and specificity of ultrasound to diagnose mineralizations; however, inconsistencies in the appearance of twinkling have led researchers to search for strategies to improve twinkling, such as modifying respiratory gases.[11] On kidney stones in pigs (implanted) and humans (naturally occurring), breathing oxygen (O_2) was found to increase twinkling, whereas pigs breathing carbon dioxide (CO_2) was found to decrease twinkling.[12,13]

These results suggest that urine and kidney stones are sensitive to changes in respiratory gases. However, O_2 and CO_2 levels in the pig urine did not track as expected based on the gas the pigs inhaled, so it is unclear which gases were present on the kidney stone.

Understanding how and where bubbles can form on different mineralizations is also important to understanding how twinkling might be influenced by changing ambient gases. Previous theoretical studies suggest that microscopic crevices can act as nucleation sites for cavitation bubbles by stabilizing gas pockets against dissolution.[14-16] More recent experimental work shows that micron sized crevices etched into solid structures can stabilize bubbles for interaction with driving ultrasound fields.[17] Crevice microbubbles have been visualized directly and indirectly on the surface of and inside kidney stones using lithotripter pulses to enlarge bubbles along with high-speed photography, environmental scanning electron microscopy (ESEM), and micro-computed tomography (μCT).[6,18] Unlike kidney stones which are often composed of many chemicals held together by an organic mesh, other pathological mineralizations are primarily composed of a single chemical with limited organic material.[4] Therefore, identifying features on crystals that could harbor bubbles is important towards understanding twinkling on pathological mineralizations.

In this paper, cholesterol, calcium phosphate, and uric acid crystals were grown *in vitro* and imaged with SEM and μCT to examine features that could harbor stable microbubbles. The same crystals were exposed to elevated levels of CO_2, O_2, and N_2 while imaging with Doppler ultrasound to investigate the effect of each gas on twinkling. We hypothesize that twinkling on all crystals will increase in elevated O_2 and decrease in elevated CO_2 but will be unaffected by

elevated N_2 levels. Additionally, we hypothesize that cholesterol will have the most surface crevices and internal pores that can harbor bubbles.

II. MATERIALS AND METHODS

A. Crystal growth

Cholesterol, calcium phosphate, and uric acid crystals, all commonly found in pathological mineralizations, were grown according to Rokni et al. (2023).[7] In brief, supersaturated solutions of each chemical were brought to a specific pH and temperature to allow for crystal nucleation and aggregation. For calcium phosphate and uric acid crystals, the pH was adjusted using 0.1 M sodium hydroxide (Belle Chemical, Billings, MT, USA) and measured with an EcoSense® pH 10A meter (YSI, Yellow Springs, OH, USA). Wooden hemispheres (diameter = 1 cm) or carbon fiber rods (diameter = 2 mm) were added to the uric acid solution for a controlled nucleation site. Crystal composition was confirmed using Raman Spectroscopy (Horiba Labram HR evolution, Kyoto, Japan).

B. Evaluating crystal microstructure

Two representative crystals of each composition were imaged with an SEM (FEI Quanta 250, Philips, Amsterdam, Netherlands) at 20 kV to evaluate surface microstructure. All SEM images were analyzed with ImageJ (NIH, Bethesda, MD, USA). The surface area and number of crevices over two representative portions of each crystal were measured using the method described by Hojat et al. (2023).[19] Briefly, a threshold was applied to the image to segment the crevices from the surrounding crystal. The image was then binarized and morphologically filtered using *Dilate* or *Erode* in ImageJ to separate individual crevices, which were verified manually. Finally, the *Analyze Particles* tool was used to extract all crevice sizes (Fig. 1).

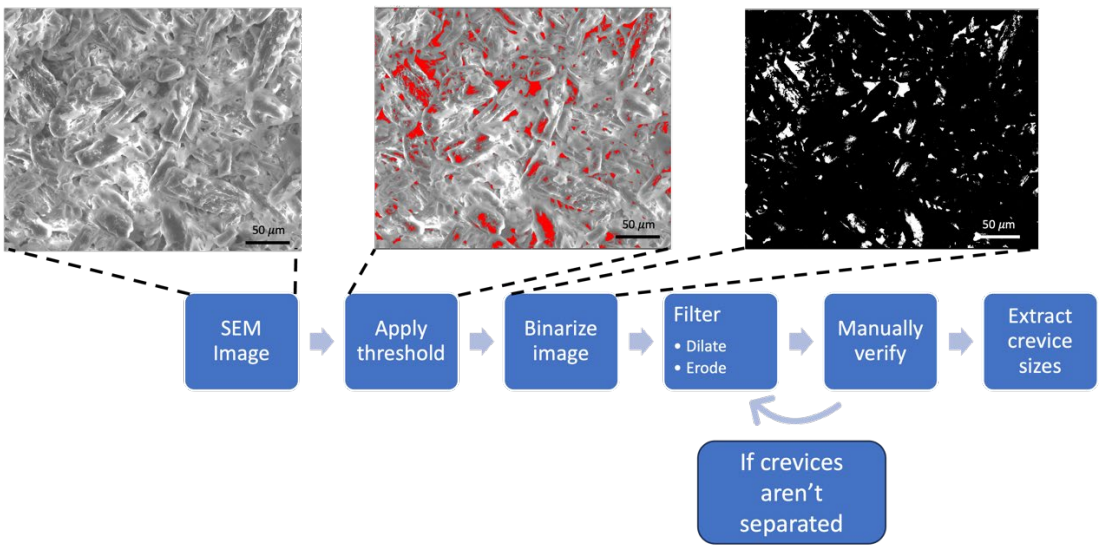

Fig. 1. Flowchart describing the image processing used to segment crevices from SEM images.

One other representative crystal of each composition was imaged with µCT. Calcium phosphate and cholesterol crystals were imaged underwater with a v|tome|x L300 machine (8 µm voxel size; GE, Boston, NY, USA). For finer resolution, uric acid crystals grown on carbon fiber rods were imaged in air with an Xradia 620 Versa machine (1.2 µm voxel size; ZEISS, Oberkochen, Germany). Single µCT slices were saved using ImageJ while internal pore volumes were calculated using Avizo® (ThermoFisher Scientific, Waltham, MA, USA). A median filter was applied to reduce noise and scans were segmented into 'crystal' and 'pore' based on thresholds set by the density of the surrounding environment. Only relative density values were necessary to differentiate pores so the µCT machines were not calibrated to give an absolute color scale.

C. Evaluating the effect of gases on twinkling

All Doppler ultrasound imaging was performed using a Verasonics® research ultrasound system (Vantage-128, Verasonics®, Kirkland, WA, USA) with an L7-4 transducer (Philips/ATL, Bothell, WA, USA; flash mode, elevation focus of 30 mm, and -6 dB azimuthal angle of 1.7°). The

pulsing scheme consisted of 7 Doppler ensembles with 12 cycles each at a center frequency of 5.2 MHz repeated at 3 kHz. This transducer and frequency were chosen to provide the best tradeoff between twinkling and resolution.[18] For the Doppler transmit voltage of 28.3 V, the Doppler waveform was measured in degassed and deionized water using a golden capsule hydrophone (HGL-Series, Onda, Sunnyvale, CA, USA) and was found to have maximum peak Doppler pressures of $p_+ \approx 3.6$ MPa and $p_- \approx 3.1$ MPa. Doppler settings were consistent between the same crystal but varied slightly ($\pm$0.3 MPa) between crystal types to ensure maximum Doppler signal without saturation. The Doppler in-phase quadrature (IQ) data was saved for analysis at ~1.5 fps.

Doppler ultrasound imaging was performed on five crystals of each composition. Crystals of the same composition were chosen to have similar maximum dimensions (cholesterol crystals ≈ 10 mm, calcium phosphate crystals ≈ 5 mm, uric acid crystals ≈ 0.3 mm grown on 8 mm wooden balls). Before imaging, crystals were submerged in water for >1 week and degassed in a desiccant chamber at ~0.01 MPa absolute for >2 hours prior to imaging. As a control, crystals were initially imaged in filtered (>5 μm) deionized water initially degassed to <2 mg/L dissolved O_2 concentration (Extech 407510 Dissolved Oxygen Meter, Extech, Waltham, MA, USA), <12 mg/L CO_2 (MI-720 Micro-Carbon Dioxide Electrode, Microelectrodes Inc., Bedford, NH, USA), and <4 mg/L dissolved nitrate (Thomas Brand Nitrate Ion Electrode, Thomas Scientific, Swedesboro, NJ, USA). To increase the concentration of O_2 and CO_2, the respective gas was bubbled through the water (Fig. 2a). O_2 was added to the water in 5 intervals to reach concentrations of 200 mg/L. In separate experiments, CO_2 was added in 5 intervals to produce concentrations of 11-125 mg/L. At each interval, crystals were allowed to reach equilibrium for

>20 min (i.e. scans produced repeatable results) and then imaged at the same location while saving IQ data for 1 min. To image crystals in elevated N_2, water was pressurized with nitrogen in a custom pressure chamber (Fig. 2b).[7] First, the water was pressurized to ~0.8 MPa absolute using nitrogen. After returning to ambient conditions, nitrate levels were continuously measured to approximate dissolved N_2 while saving to the computer at 1 point per second (pHenomenal MU1600H, VWR, Radnor, PA, USA). Nitrate levels were measured instead of actual dissolved N_2 as no probes exist to directly measure N_2. Simultaneously, crystals were imaged with Doppler ultrasound for 2 min while saving IQ data, which allowed for direct comparison between dissolved N_2 levels and twinkling. At least 15 min after dissolved N_2 returned to the original levels, crystals were again imaged in the same location while saving IQ data for 1 min as the control. For all changes in gas, twinkling on each crystal was calculated by summing the Doppler power within a region of interest (ROI) box around the crystal. To allow for comparison between crystal types, the Doppler power was normalized by dividing the mean Doppler power across each crystal type at every gas interval by the mean Doppler power of the control (i.e. <2 mg/L O_2, <12mg/L CO_2, <4 mg/L nitrate).

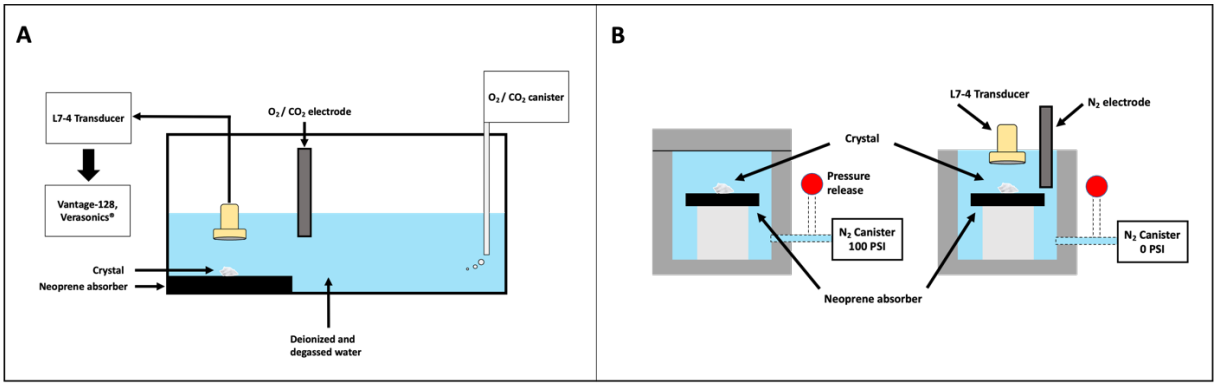

Fig. 2 (a) Experimental arrangement for increasing dissolved O_2 or CO_2 concentrations in water while imaging crystals with Doppler ultrasound. (b) Experimental arrangement for increasing

dissolved N_2 concentrations prior to imaging crystals. Water was pressurized with N_2 (left) and crystals were imaged after the pressure was released (right).

D. Statistical analysis

All statistical analyses were performed using Minitab (Minitab, State College, PA, USA). A Ryan-Joiner test was used to check all distributions for normality. Internal pore sizes were compared using a Kruskal-Wallis test with post-hoc Dunn tests. One-way ANOVAs and post-hoc Dunnett tests were used to compare the effect of each gas on twinkling to the control. Values of $p<0.05$ indicate statistical significance.

III. RESULTS

A. Evaluating crystal microstructure

All crystals imaged with SEM contained many crevices that could harbor stable bubbles (Fig. 3a-c). Across a surface area of ~0.16 mm^2, cholesterol crystals had ~1300 crevices with a median crevice area of 3.80 μm^2 (IQR = 11.25 μm^2). These crevices were described as deep as the bottom of the crevices were not visible on the SEM image. Across the same surface area of ~0.16 mm^2, calcium phosphate crystals had ~1200 crevices with a median crevice area of 4.34 μm^2 (IQR = 10.98 μm^2). These crevices were described as shallow as the bottom of all these crevices were visible on the SEM image. Across the same surface area of ~0.16 mm^2, uric acid crystals had ~500 crevices, mostly in between individual crystals, with a median crevice area of 4.83 μm^2 (IQR = 12.68 μm^2). These crevices were of mixed depths, as only some of the crevice bottoms could be viewed on the SEM images. The distribution of crevice sizes for all crystals was not normally distributed ($p<0.01$) as ~70% of all crevices fell below 10 μm^2 (Fig. 3d).

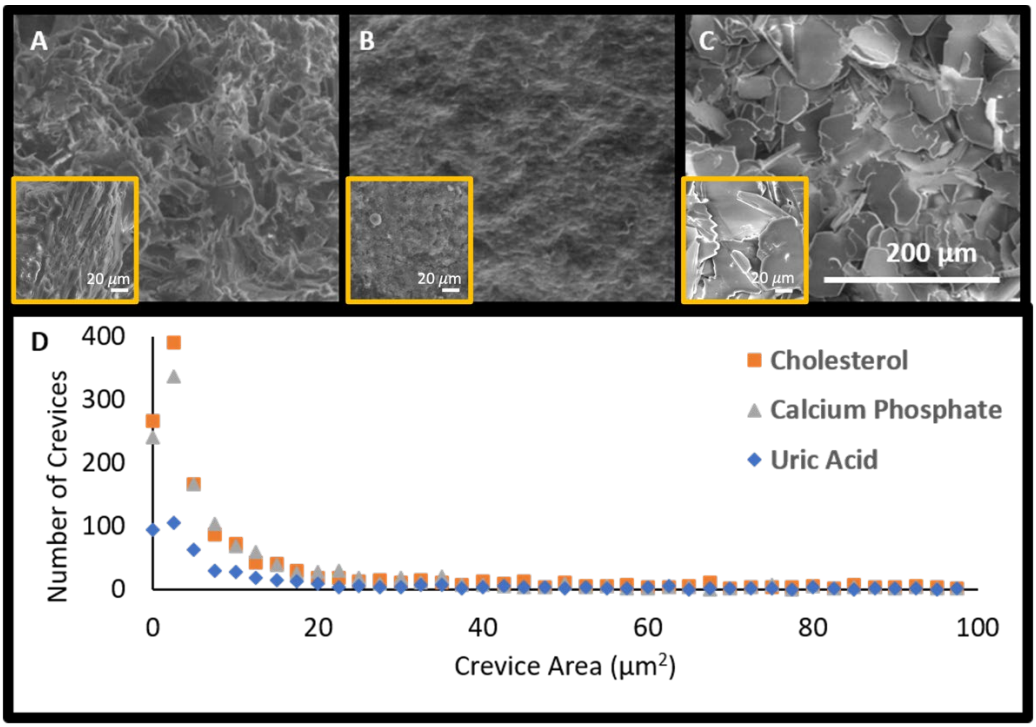

Fig. 3. (color online) Representative scanning electron microscopy images of (A) cholesterol, (B) calcium phosphate, and (C) uric acid. Zoomed in portions of each crystal are presented in the lower left corner with the yellow border. (D) A histogram comparing the number and area of crevices for each crystal type.

The internal structures noted on the µCT scans varied drastically between crystal types (Fig. 4a-c). The distributions of pore volumes for all crystals were not normally distributed ($p<0.01$). Cholesterol had 117 pores with a median volume of 41000 μm^3 (IQR= 139000 μm^3) that ran throughout the entire volume of the crystal. Calcium phosphate had 141 pores with a median volume of 2600 μm^3 (IQR = 6000 μm^3) which primarily appeared as cracks along the edges of the crystal. Uric acid had 1262 pores with a median volume of 3.78×10^{-9} μm^3 (IQR = 4.34×10^{-8} μm^3). The median pore size in cholesterol was significantly larger than in calcium phosphate ($p=0.002$) which was significantly larger than in uric acid ($p<0.001$) (Fig. 4d).

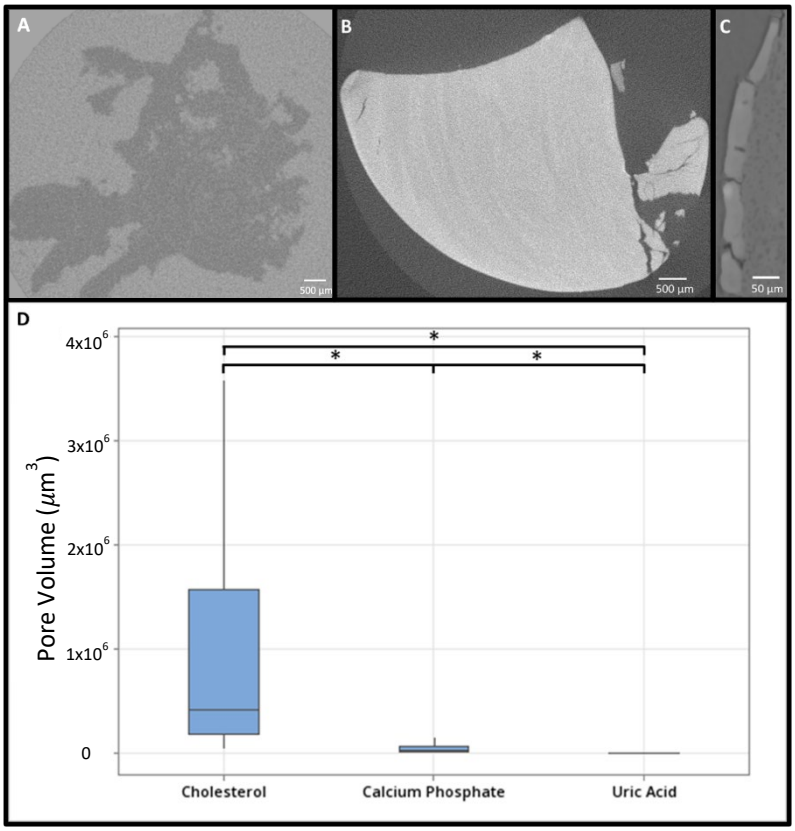

Fig. 4. (color online) Representative slices from micro-computed tomography images of (A) cholesterol, (B) calcium phosphate, and (C) uric acid. Internal pore volumes were calculated from full three-dimensional rendering of the crystal. (D) A box-plot of pore volumes for each crystal composition.

B. Evaluating the effect of gases on twinkling

Imaging crystals in elevated O_2 significantly increased twinkling on cholesterol crystals ($p<0.001$) when the dissolved O_2 concentration exceeded 9 mg/L; twinkling remained unchanged on calcium phosphate ($p=0.92$) and uric acid ($p=0.41$) crystals (Fig. 3a). Imaging crystals in elevated CO_2 significantly increased twinkling on cholesterol ($p<0.001$) and uric acid ($p=0.009$) crystals when the dissolved CO_2 concentration exceeded 55 mg/L; the increase in Doppler power on uric acid crystals was not significantly different from 79 – 103 mg/L ($p=0.88$

and p=0.28, respectively), but was again significant at 125 mg/L (p=0.01). Twinkling remained unchanged on calcium phosphate crystals (p=0.82) (Fig. 3b). Imaging crystals in elevated N_2 caused no changes in twinkling for cholesterol (p=0.23), calcium phosphate (p=0.44), or uric acid (p=0.81) crystals (Fig. 3c).

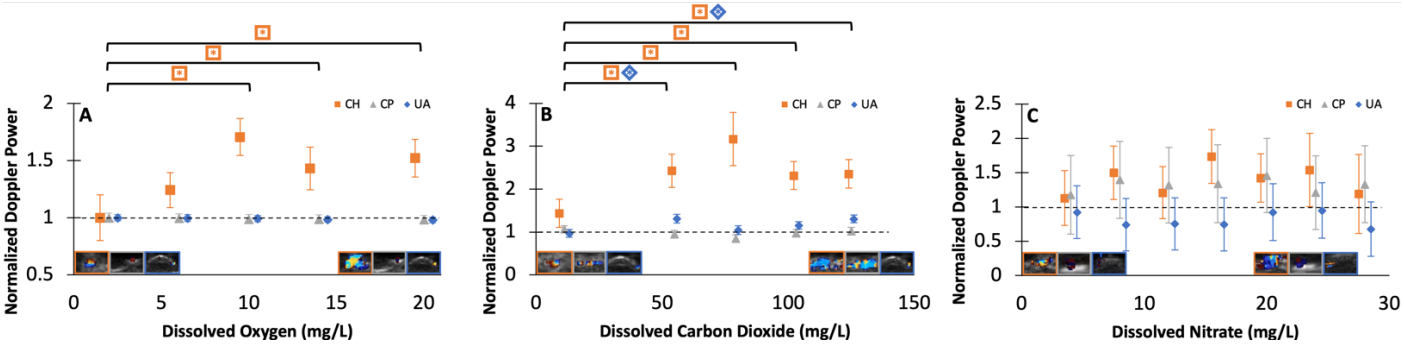

Fig. 5. (color online) Plots of dissolved gas concentration versus mean Doppler power normalized to control for (A) oxygen, (B) carbon dioxide, and (C) nitrate. Representative twinkling images are given for the control (left) and at the third data point (right) for each crystal type and gas. The color around the twinkling image indicates which crystal is shown with cholesterol, calcium phosphate, and uric acid presented left to right. Statistical significance (ANOVA, $p<0.05$) compared to control is indicated by an asterisk related to the respective shape and color.

IV. DISCUSSION

These results provide evidence supporting the crevice microbubble theory of twinkling as ambient gases affect twinkling on crystals. Elevated O_2 increased twinkling for cholesterol crystals with no change for calcium phosphate or uric acid crystals. Increasing CO_2 increased twinkling for cholesterol and calcium phosphate crystals with no change in twinkling for uric acid crystals. Increasing N_2 did not change twinkling for any of the tested crystal types. SEM

images show each crystal has unique surface characteristics that can harbor microbubbles. μCT images show cracks and pores throughout the crystals that could contain gas. Cholesterol crystals had the most and deepest surface crevices and the largest internal pore volumes compared to calcium phosphate and uric acid crystals. Although changing the concentration of the gas in the surrounding water most likely affected the presence of bubbles on the surface of the crystals, it is possible that internal bubbles may have also been affected through internal pores connected to the surface or by diffusing through the solid.

From the SEM and μCT scans, cholesterol crystals were found to have the most features suitable for bubbles to form. This observation agrees with our previous work that shows twinkling is strongest on cholesterol crystals, followed by calcium phosphate and uric acid crystals.[7] Additionally, all crystal types had the most crevices with areas ranging from 0-5 μm^2 which generally aligned with crevice sizes noted on kidney stones.[18] For the SEM scans, only a small portion of the crystal surface was imaged due to limits in the technology so variations in the surface could be present that are not accounted for in these analyses. Moreover, while SEM methods exist to measure crevice depth by imaging at two different angles, due to time and equipment restraints these additional measurements were not performed. Crevice volumes could be substantially different than the reported surface areas. For μCT, only a single crystal of each composition due to cost and machine scheduling; it is likely that some variations in the internal structure will exist across crystals of the same composition, although this variation is expected to be small as growing conditions were similar for all tested crystals of the same composition. While no obvious gas pockets were visible in crystals scanned underwater with μCT, it is possible any bubbles present were smaller than the minimum resolvable features.

Future µCT scans while pulling vacuum on the crystals could allow for visualization of internal microbubbles. It is important to note that there are differences in the size and growing conditions of these crystals compared to pathological mineralizations that could differentiate these results from what would happen *in vivo.*

Increasing the gas concentration around crystals caused the biggest increase in twinkling for cholesterol crystals in O_2 and CO_2. This result is supported by the SEM and µCT images which showed that cholesterol had more external and internal features that could harbor microbubbles compared to calcium phosphate and uric acid crystals. In addition, it is well known that hydrophobic impurities can act to stabilize bubbles.[20] As cholesterol is the most hydrophobic of the tested crystals, it is possible more bubbles are present on cholesterol crystals than calcium phosphate or uric acid, resulting in more twinkling.[2,21] These results differ from previous studies with natural and implanted *in vivo* kidney stones which found that twinkling increased when patients breathed O_2 and decreased when patients breathed CO_2.[12,13] Biological adaptations to the changing gases are likely to affect bubble formation *in vivo* and could explain the differences between studies.[22] For example, the kidney compensates for increases in CO_2 by scavenging O_2 from the urine, whereas other organs may remain acidotic when exposed to high levels of CO_2.[23-25] Finally, there was no effect of N_2 on any of the stones. N_2 is nearly inert and difficult to dissolve into solution so it was expected that elevated levels of N_2 would have little effect on twinkling. The higher variation noted with N_2 gas is likely a consequence of using the pressure chamber to increase the N_2 making it difficult to produce consistent changes in twinkling.

As N_2 could not be measured directly, it is likely that measuring nitrate underestimates the total dissolved N_2 as nitrite or ammonia could also be present in the solution, which would overemphasize the already small effect that N_2 had on twinkling. Although the system was allowed to reach equilibrium before scanning, it is possible that the gases did not diffuse completely into the crevices. The ultrasound transducer and frequency were held constant to allow for direct comparison. However, as twinkling is affected by frequency[18] and the size of the wavelength in relation to the crevice bubbles, further studies are necessary to investigate whether changing the frequency would affect these results. Finally, normal oxygen levels range from ~4-6 mg/L while breathing in pure oxygen can increase the concentration to ~20 mg/L in pigs.[12] Normal carbon dioxide levels range from ~60-90 mg/L while elevated carbon dioxide levels, which can be found in space, can increase the concentration to ~190 mg/L.[12] Normal serum nitrate levels range from 0.6 to 4.6 mg/L.[26] However, treatments with nitrates are common for cardiac disease, can cause serum levels to reach 18 mg/L or higher.[27] Therefore, the tested ranges are physiologically possible and could be leveraged to enhance twinkling.

V. CONCLUSION

These results continue to support the theory that microbubbles are present on crystals and cause twinkling. Imaging crystals with SEM and μCT provided visual evidence of features that could harbor stable microbubbles and supported our previous result that cholesterol crystals twinkle more than calcium phosphate and uric acid crystals. Elevated O_2 caused twinkling to increase on cholesterol crystals, elevated CO_2 increased twinkling on cholesterol and calcium phosphate crystals, and elevated N_2 caused no change in twinkling. These results

suggest varying ambient gases could be used to enhance twinkling and improve detection of some pathological mineralization compositions.

ACKNOWLEDGMENTS

The authors would like to acknowledge Andrew Ross, Kenneth Meinert Jr., and America Campillo from the Energy and Environmental Sustainability Laboratories at Penn State, Center for Quantitative Imaging for performing the μCT scans and assisting with data interpretation. The authors would also like to acknowledge Julie Anderson of The Penn State Materials Characterization Lab for assistance performing and interpreting the SEM scans. This work was supported by the National Science Foundation CAREER Grant No. 1943937 and the NSF Graduate Research Fellowship Program DGE1255832.

AUTHOR DECLARATIONS

Conflict of Interest

The authors have no conflicts to disclose.

DATA AVAILABILITY

The data that support the findings of this study are available from the corresponding author upon reasonable request.

REFERENCES

[1]E. Pascual and F. Sivera, "Crystal analysis in synovial fluid," Curr Opin Rheumatol, **23**(2), 161-169 (2011).

[2]A. Grebe and E. Latz, "Cholesterol crystals and inflammation," Curr Rheumatol Rep **15,** 313 (2013).

[3]B. Mujtaba, A. Taher, M. J. Fiala, S. Nassar, J. E. Madewell, A. K. Hanafy, and R. Aslam, "Heterotopic ossification: radiological and pathological review," Radiol Oncol **53**(3), 275-284 (2019).

[4]E. Tsolaki and S. Bertazzo, "Pathological mineralizations: the potential of mineralomics," Materials **12,** 3126 (2019).

[5]W. Lu, O. A. Sapozhnikov, M. R. Bailey, P. J. Kaczkowski, and L. A. Crum, "Evidence for Trapped Surface Bubbles as the cause for the twinkling artifact in ultrasound imaging," Ultrasound Med Biol **39**(6), 1026-1038 (2013).

[6]J. C. Simon, O. A. Sapozhnikov, W. Kreider, M. Breshock, J. C. Williams, and M. R. Bailey, "The role of trapped bubbles in kidney stone detection with the color Doppler ultrasound twinkling artifact," Phys Med Biol **63**(2), 025011 (2018).

[7]E. Rokni and J. C. Simon, "The effect of crystal composition and environment on the color Doppler ultrasound twinkling artifact," Phys. Med. Biol. **68**, 035021 (2023).

[8]A. Rahmouni, R. Bargoin, A. Herment, N. Bargoin, and N. Vasile, "Color Doppler twinkling artifact in hyperechoic regions," Radiology **199**(1), 269-271 (1996).

[9]D. V. Leonov, N. S. Kulberg, A. I. Gromov, and S. P. Morozov, "Detection of microcalcifications using the ultrasound Doppler twinkling artifact," Biomedical Engineering **54**(3), 174-178 (2020). Translated from Meditsinskaya Tekhnika **54**(3), 14-17 (2020).

[10]H. C. Kim, D. M. Yang, W. Jin, J. K. Ryu, H. C. Shin, "Color Doppler twinkling artifacts in various conditions during abdominal and pelvic sonography," J Ultrasound Med **29**(4), 621-632 (2010).

[11]S. J. Park, B. H. Yi, H. K. Lee, Y. H. Kim, G. J. Kim, and H. C. Kim, "Evaluation of patients with suspected ureteral calculi using sonography as an initial diagnostic tool: how can we improve diagnostic accuracy?" J Ultrasound Med **7**, 1441-1450 (2008).

[12] J. C. Simon, Y. Wang, B. W. Cunitz, J. Thiel, F. Starr, Z. Liu, and M. R. Bailey, "The effect of carbon dioxide on the twinkling artifact in ultrasound imaging of kidney stones: A pilot study," Ultrasound Med Biol **43**(5), 877-883 (2017).

[13]J. C. Simon, J. R. Holm, J. Thiel, B. Dunmire, B. W. Cunitz, M. R. Bailey, "Evidence of microbubbles on kidney stones in humans," Ultrasound Med Biol **46**(7), 1802-1807 (2020).

[14]L. Crum, "Tensile strength of water," *Nature* **278**, 148-149 (1979).

[15]R. E. Apfel, "The role of impurities in cavitation-threshold determination," *J Acoust Soc Am* **48**(5), 1179-1186 (1970).

[16]A. A. Atchley and A. Prosperetti, "The crevice model of bubble nucleation," *J Acoust Soc Am* **86**(3), 1065-1084 (1989).

[17]A. Ziljstra, D. F. Rivas, H. J. G. E. Versluis, D. Lohse, "Enhancing acoustic cavitation using artificial crevice bubbles," *Ultrasonics* **56**, 512-523 (2015).

[18] E. Rokni, S. Zinck, and J. C. Simon, "Evaluation of stone features that cause the color Doppler ultrasound twinkling artifact," Ultrasound Med Biol **47**(5), 1310-1318 (2021).

[19]N. Hojat, P. Gentile, A. M. Ferreira, L. Šiller, "Automatic pore size measurements from scanning electron microscopy images of porous scaffolds," J Porous Mater **30**, 92-101 (2023).

[20]F. S. Rawnaque and J. C. Simon, "The effect of elastic modulus and impurities on bubble nuclei available for acoustics cavitation in polyacrylamide hydrogels," J Acoust Soc Am **152**, 3502-3509 (2022).

312 [21]J. T. Carstensen, C. Ertell, “Physical and chemical properties of calcium phosphates for solid
313 state pharmaceutical formulations,” Drug Dev Ind Technol **94**, 96-104 (1983).
314 [22]J. E. Blatteau, J. B. Souraud, E. Gempp, and A. Boussuges, “Gas nuclei, their origin, and their
315 role in bubble formation,” Aviation Space Environ Med **77**, 1068-1076 (2006).
316 [23]P. Hansell, W. J. Welch, R. C. Blantz, and F. Palm, “Determinants of kidney oxygen
317 consumption and their relationship to tissue oxygen tension in diabetes and hypertension,”
318 Clin Exp Pharmacol Physiol **40**(2), 123-137 (2013).
319 [24]J. Collins, A. Rudenski, J. Gibson, L. Howard, and R. O’Driscoll, “Relating oxygen partial
320 pressure, saturation and content: the haemoglobin-oxygen dissociation curve,” Breathe **11**(3),
321 194-201 (2015).
322 [25]D. A. Kregenow and E. R. Swenson, “The lung and carbon dioxide: implications for permissive
323 and therapeutic hypercapnia,” Eur Resp J **20**, 6-11 (2002).
324 [26]A. Ghasemi, S. Zahediasl, and F. Azizi, “Reference values for serum nitric oxide metabolites in
325 an adult population,” Clin Biochem **43**, 89-94 (2010).
326 [27]Y. Ersoy, E. Özerol, Ö. Baysal, I. Temel, R. S. MacWalter, Ü. Meral, and Z. E. Altay, “Serum
327 nitrate and nitrite levels in patients with rheumatoid arthritis, ankylosing spondylitis, and
328 osteoarthritis,” Ann Rheum Dis **61**, 76-78 (2002).
329